


## Article

# A General Model for Analyzing the Unsteady Pressure Performance of Composite Gas Reservoirs

Yu Huang <sup>1,\*</sup> , Mingfeng Ma <sup>1</sup>, Xin Wang <sup>1</sup> and Xiaoping Li <sup>2,\*</sup><sup>1</sup> College of Safety Engineering, Chongqing University of Science & Technology, Chongqing 401331, China<sup>2</sup> State Key Laboratory of Oil and Gas Reservoir Geology and Exploitation, Southwest Petroleum University, Chengdu 610500, China

\* Correspondence: huangyu\_swpu@163.com (Y.H.); lixiaoping\_swpu@163.com (X.L.)

**Abstract:** Based on the previous study of a single medium model, the dual medium model for the fractured composite reservoir and the triple medium model for a fracture–cavity composite reservoir was established, respectively. The similarities and differences in the corresponding pressure dynamic curves of each model were analyzed, and the general model of a composite gas reservoir composed of different inner and outer zones was obtained. The general model can be more easily used in actual production, and the accuracy and practicability of the model were verified by case analysis.

**Keywords:** general model; fluid flow; percolation; composite reservoir



**Citation:** Huang, Y.; Ma, M.; Wang, X.; Li, X. A General Model for Analyzing the Unsteady Pressure Performance of Composite Gas Reservoirs. *Energies* **2022**, *15*, 8362. <https://doi.org/10.3390/en15228362>

Academic Editors: Hongfang Lu, Enbin Liu, Shanbi Peng and Chengyong Li

Received: 11 October 2022

Accepted: 7 November 2022

Published: 9 November 2022

**Publisher's Note:** MDPI stays neutral with regard to jurisdictional claims in published maps and institutional affiliations.



**Copyright:** © 2022 by the authors. Licensee MDPI, Basel, Switzerland. This article is an open access article distributed under the terms and conditions of the Creative Commons Attribution (CC BY) license (<https://creativecommons.org/licenses/by/4.0/>).

## 1. Introduction

With the great attention paid to carbon emission by various countries [1], carbonate reservoirs, as an important member of the “carbon sink effect”, have also become a research hotspot. In actual production, formation acidification or reservoir characteristics will result in formation parameters near the wellbore that are different from those away from the wellbore. This type of reservoir is called a composite reservoir, while carbonate reservoirs contain fractures and caves, and the reservoirs are mostly dual or triple medium, so their composite characteristics will be more complex than conventional reservoirs.

Our previous research work mainly introduced the unstable dynamic characteristics of a composite reservoir with a single medium both in the inner zone and outer zone [2]. However, the roles played by fractured reservoirs and fracture–cavity reservoirs in oil and gas production are becoming increasingly important. Therefore, it is significant to study the unstable dynamics of these two types of reservoirs.

However, studies have rarely considered both the composite formation in the dual or triple medium. Stress sensitivity refers to the properties of the reservoir that change with the effective pressure, and permeability stress sensitivity has a much greater impact on the production performance than the porosity stress sensitivity [3]. Therefore, when the percolation theory is involved in stress sensitivity, it usually means the permeability stress sensitivity. Pedrosa (1986) found that stress sensitivity has a great influence on the well performance [4]. Warren and Root (1963) established the Warren–Root model to study the characteristics of fracture–matrix reservoirs, and the matrix is considered as the source of fractures, and fractures are the only access to the wellbore [5]. In 1975, Clossman set up the triple–porosity model on the basis of the dual–porosity model (Warren–Root model) for the first time. The matrix and cave are the source, and fracture is still the only way to enter the wellbore [6]. Jiang et al. (2020) established an unstable seepage model for fractured straight wells considering the stress sensitivity effect, and analyzed the transient pressure characteristics of fractured wells under different reservoir medium combinations [7]. Jing et al. (2022) analyzed the cross flow characteristics between adjacent formations in multi-layer reservoirs, and evaluated the influence of formation characteristics on the pressure behavior away from the well circumference [8]. Zhao et al. (2013) and Guo et al. (2015),

respectively, provided “three-medium” and “four-medium” models to study the rate characteristics of shale gas reservoirs [9,10]. Chen et al. (2017) analyzed the influence of the fractured–vuggy cave size and the distance between the fractured–vuggy cave and well on the bottom hole pressure response curve by the finite element method [11].

Although some researchers have studied the seepage mechanism of triple-porosity reservoirs, these studies did not consider the characteristics of composite reservoirs.

Wei et al. (2021) established a composite reservoir seepage model of dual medium under the influence of different outer boundaries by introducing fractal theory, and affirmed the application of a similar structure method in solving complex reservoir models [12]. Fankun et al. (2019) analyzed the percolation characteristics of carbonate composite reservoirs with triple medium in the inner area and single media in the outer area, and the main channel in the inner area is fracture [13]. Zhao et al. (2016) and Wu et al. (2017) discussed the characteristics of transient pressure type curves for the fractured horizontal well in arbitrary shaped composite reservoirs by using the boundary element method [14,15]. Zhu et al. (2017) built a composite seepage model that considered the stress sensitivity and a rectangle dual-porosity inner zone to investigate the pressure transient response of a vertically fractured well [16]. Wang et al. (2018) discussed the characteristics of production decline for vertical wells and verified the results through numerical methods. However, the object of this study was a vertical well and did not consider the stress sensitivity effect [17].

At present, although the research on composite reservoirs has gradually deepened, most of the studies have not taken complex media, or composite reservoir and reservoir stress sensitivity are considered uniformly. Moreover, the reservoir conditions of different reservoirs are not the same, so it is not convenient to combine the theoretical model with practical application.

Therefore, on the basis of the single medium model, dual medium and triple medium models were established, respectively, and a general model was established by summarizing the characteristics of each model. The new model is more flexible and more convenient for practical application.

Since the single medium model has been published, it will not be repeated here. For details, please refer to the article “Transient Pressure and Rate Decline Analysis for Horizontal Well in Stress-Sensitive Composite Reservoir” [2].

## 2. Materials and Methods

### 2.1. Dual Medium Model of Composite Gas Reservoir

#### 2.1.1. Physical Model

The dual-porosity medium is characterized by the Warren–Root model. The fracture is the only channel for gas to wellbore, the physical properties of reservoirs in the inner and outer zone are different, but both are dual medium.

Other assumptions are consistent with Section 2.1 in [2]. The physical model is shown in Figure 1.

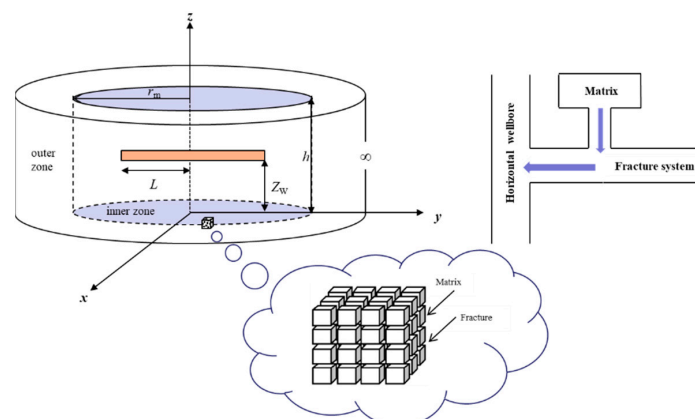


**Figure 1.** Physical model of the dual-porosity medium.

### 2.1.2. Mathematical Model

Continuity equations are as follows:

$$\begin{cases} \frac{\partial(\rho_f \varphi_f)}{\partial t} + \nabla \cdot (\rho \vec{v}_f) - q_{ex} = 0 \\ \frac{\partial(\rho_m \varphi_m)}{\partial t} + q_{ex} = 0 \end{cases} \tag{1}$$

Interporosity flow equations:

$$q_{ex} = \frac{3.6\alpha K_m \rho_0}{\mu} (p_m - p_f) \tag{2}$$

The equation of motion after considering the stress sensitivity is as follows:

$$\begin{cases} v_{fr} = -3.6 \frac{K_{fh}}{\mu} e^{-\gamma(p_i - p_f)} \frac{\partial p_f}{\partial r} \\ v_{fz} = -3.6 \frac{K_{fv}}{\mu} e^{-\gamma(p_i - p_f)} \frac{\partial p_f}{\partial z} \end{cases} \tag{3}$$

Introducing the formula of pseudo pressure Equation (4), and the formula of permeability modulus defined by fracture pseudo pressure Equation (5):

$$\begin{cases} m_f = \int_{p_0}^{p_f} \frac{2p}{\mu Z} dp \\ m_m = \int_{p_0}^{p_m} \frac{2p}{\mu Z} dp \end{cases} \tag{4}$$

$$K_{fh} = K_i e^{-\gamma(m_i - m_f)} \tag{5}$$

Introducing the dimensionless expression in Table 1, the dimensionless dual medium model of a composite reservoir can be obtained:

Inner zone ( $0 \leq r_D \leq r_{mD}$ ):

$$\begin{cases} \frac{1}{r_D} \frac{\partial}{\partial r_D} \left( r_D \frac{\partial m_{f1D}}{\partial r_D} \right) - \gamma_{mD} \left( \frac{\partial m_{f1D}}{\partial r_D} \right)^2 + L_D^2 \left[ \frac{\partial^2 m_{f1D}}{\partial z_D^2} - \gamma_{mD} \left( \frac{\partial m_{f1D}}{\partial z_D} \right)^2 \right] \\ = e^{\gamma_{mD} m_{f1D}} \left[ \omega_1 \frac{\partial m_{f1D}}{\partial t_D} + (1 - \omega_1) \frac{\partial m_{m1D}}{\partial t_D} \right] \\ (1 - \omega_1) \frac{\partial m_{m1D}}{\partial t_D} + \lambda_1 (m_{m1D} - m_{f1D}) = 0 \end{cases} \tag{6}$$

Outer zone ( $r_{mD} \leq r_D < \infty$ ):

$$\begin{cases} \frac{1}{r_D} \frac{\partial}{\partial r_D} \left( r_D \frac{\partial m_{f2D}}{\partial r_D} \right) + L_D^2 \frac{\partial^2 m_{f2D}}{\partial z_D^2} = \eta_{II} \left[ \omega_2 \frac{\partial m_{f2D}}{\partial t_D} + (1 - \omega_2) \frac{\partial m_{m2D}}{\partial t_D} \right] \\ \eta_{II} (1 - \omega_2) \frac{\partial m_{m2D}}{\partial t_D} + \lambda_2 (m_{m2D} - m_{f2D}) = 0 \end{cases} \tag{7}$$

Conditions:

$$\begin{cases} m_{fjD} |_{t_D=0} = m_{mjD} |_{t_D=0} = 0 \quad (j = 1, 2) \\ \lim_{\epsilon_D \rightarrow 0} \left[ \lim_{r_D \rightarrow 0} \int_{z_{wD} - \frac{\epsilon_D}{2}}^{z_{wD} + \frac{\epsilon_D}{2}} \left( r_D e^{-\gamma_{mD} m_{f1D}} \frac{\partial m_{f1D}}{\partial r_D} \right) dz_{wD} \right] = -\frac{1}{2} |z_D - z_{wD}| \leq \frac{\epsilon_D}{2} \\ m_{f1D} |_{r_D=r_{mD}} = m_{f2D} |_{r_D=r_{mD}} \\ \frac{\partial m_{f1D}}{\partial r_D} |_{r_D=r_{mD}} = \frac{1}{M_{12}} \frac{\partial m_{f2D}}{\partial r_D} |_{r_D=r_{mD}} \\ m_{f2D} |_{r_D \rightarrow \infty} = m_{m2D} |_{r_D \rightarrow \infty} = 0 \\ \frac{\partial m_{fjD}}{\partial z_D} |_{z_D=0,1} = \frac{\partial m_{mjD}}{\partial z_D} |_{z_D=0,1} = 0 \quad (j = 1, 2) \end{cases} \tag{8}$$

**Table 1.** Dimensionless variables of the dual medium model.

Variable	Equation (j = 1,2)	Variable	Equation (j = 1,2)
Fracture pseudo pressure	$m_{fjD} = \frac{78.489K_{fh1}h}{Tq_{sc}} (m_i - m_{fj})$	Permeability modulus	$\gamma_{mD} = \frac{Tq_{sc}}{78.489K_{fh1}h} \gamma_m$
Matrix pseudo pressure	$m_{mjD} = \frac{78.489K_{fh1}h}{Tq_{sc}} (m_i - m_{mj})$	Storage coefficient	$C_D = \frac{0.159C}{(\phi_{f1}C_{f1} + \phi_{m1}C_{m1})hL^2}$
Storage ratio	$\omega_j = \frac{\phi_{fj}C_{fj}}{\phi_{fj}C_{fj} + \phi_{mj}C_{mj}}$	Pressure transmitting coefficient ratio	$\eta_{II} = \frac{K_{fh1}\mu_2(\phi_{f2}C_{f2} + \phi_{m2}C_{m2})}{K_{fh2}\mu_1(\phi_{f1}C_{f1} + \phi_{m1}C_{m1})}$
Interporosity coefficient	$\lambda_j = \alpha_j \frac{K_{mj}}{K_{fhj}} L^2$	Time	$t_D = \frac{3.6K_{fh1}t}{(\phi_{f1}C_{f1} + \phi_{m1}C_{m1})\mu_1L^2}$

By introducing the Pedrosa substitution and taking the zeroth order perturbation solution, the dimensionless model can be changed into the following form:

Differential equations:

$$\left\{ \begin{array}{l} (0 \leq r_D \leq r_{mD}) \left\{ \begin{array}{l} \frac{1}{r_D} \frac{\partial}{\partial r_D} \left( r_D \frac{\partial \xi_{1D0}}{\partial r_D} \right) + L_D^2 \frac{\partial^2 \xi_{1D0}}{\partial z_D^2} \\ = \omega_1 \frac{\partial \xi_{1D0}}{\partial t_D} + (1 - \omega_1) \frac{\partial m_{m1D}}{\partial t_D} \\ (1 - \omega_1) \frac{\partial m_{m1D}}{\partial t_D} + \lambda_1 [m_{m1D} - \xi_{1D0}] = 0 \end{array} \right. \\ (r_{mD} \leq r_D < \infty) \left\{ \begin{array}{l} \frac{1}{r_D} \frac{\partial}{\partial r_D} \left( r_D \frac{\partial m_{f2D}}{\partial r_D} \right) + L_D^2 \frac{\partial^2 m_{f2D}}{\partial z_D^2} \\ = \eta_{II} \left[ \omega_2 \frac{\partial m_{f2D}}{\partial t_D} + (1 - \omega_2) \frac{\partial m_{m2D}}{\partial t_D} \right] \\ \eta_{II} (1 - \omega_2) \frac{\partial m_{m2D}}{\partial t_D} + \lambda_2 (m_{m2D} - m_{f2D}) = 0 \end{array} \right. \end{array} \right. \quad (9)$$

Conditions:

$$\left\{ \begin{array}{l} \xi_{1D0}|_{t_D=0} = m_{f2D}|_{t_D=0} = m_{mjD}|_{t_D=0} = 0 \quad (j = 1, 2) \\ \lim_{\epsilon_D \rightarrow 0} \left[ \lim_{r_D \rightarrow 0} \int_{z_{wD} - \frac{\epsilon_D}{2}}^{z_{wD} + \frac{\epsilon_D}{2}} \left( r_D \frac{\partial \xi_{1D0}}{\partial r_D} \right) dz_{wD} \right] = -\frac{1}{2} |z_D - z_{wD}| \leq \frac{\epsilon_D}{2} \\ \xi_{1D0}|_{r_D=r_{mD}} = m_{f2D}|_{r_D=r_{mD}} \\ \frac{\partial \xi_{1D0}}{\partial r_D} |_{r_D=r_{mD}} = \frac{1}{M_{12}} \frac{\partial m_{f2D}}{\partial r_D} |_{r_D=r_{mD}} \\ m_{f2D}|_{r_D \rightarrow \infty} = m_{m2D}|_{r_D \rightarrow \infty} = 0 \\ \frac{\partial \xi_{1D0}}{\partial z_D} |_{z_D=0,1} = \frac{\partial m_{f2D}}{\partial z_D} |_{z_D=0,1} = \frac{\partial m_{mjD}}{\partial z_D} |_{z_D=0,1} = 0 \quad (j = 1, 2) \end{array} \right. \quad (10)$$

Applying the Laplace transform and orthogonal transform to the model:

$$\left\{ \begin{array}{l} \frac{1}{r_D} \frac{\partial}{\partial r_D} \left( r_D \frac{\partial \bar{\xi}_{1D0}}{\partial r_D} \right) - \left[ \frac{\lambda_1 + s\omega_1(1-\omega_1)}{\lambda_1 + (1-\omega_1)s} s + n^2 \pi^2 L_D^2 \right] \bar{\xi}_{1D0} = 0 \\ \frac{1}{r_D} \frac{\partial}{\partial r_D} \left( r_D \frac{\partial \bar{m}_{f2D}}{\partial r_D} \right) - \left[ \frac{\lambda_2 + \eta_{II}s\omega_2(1-\omega_2)}{\lambda_2 + (1-\omega_2)\eta_{II}s} \eta_{II}s + n^2 \pi^2 L_D^2 \right] \bar{m}_{f2D} = 0 \\ \lim_{r_D \rightarrow 0} r_D \frac{\partial \bar{\xi}_{1D0}}{\partial r_D} = \frac{-\cos n\pi z_{wD}}{2s} \\ \bar{\xi}_{1D0}|_{r_D=r_{mD}} = \bar{m}_{f2D}|_{r_D=r_{mD}} \\ \frac{\partial \bar{\xi}_{1D0}}{\partial r_D} |_{r_D=r_{mD}} = \frac{1}{M_{12}} \frac{\partial \bar{m}_{f2D}}{\partial r_D} |_{r_D=r_{mD}} \\ \bar{m}_{f2D}|_{r_D \rightarrow \infty} = \bar{m}_{m2D}|_{r_D \rightarrow \infty} = 0 \end{array} \right. \quad (11)$$

Therefore, the corresponding pseudo pressure expression can be obtained:

$$\begin{aligned} \bar{\zeta}_{1D0} = & A_0 \int_{-1}^1 K_0(f_{10} \sqrt{(x_D - \alpha)^2}) d\alpha + B_0 \int_{-1}^1 I_0(f_{10} \sqrt{(x_D - \alpha)^2}) d\alpha \\ & + 2 \sum_{n=1}^{\infty} \left[ \begin{aligned} & A_n \int_{-1}^1 K_0(f_{1n} \sqrt{(x_D - \alpha)^2}) d\alpha \\ & + B_n \int_{-1}^1 I_0(f_{1n} \sqrt{(x_D - \alpha)^2}) d\alpha \end{aligned} \right] \cdot \cos n\pi z_D \end{aligned} \tag{12}$$

where:

$$\begin{aligned} f_{1n} = & \sqrt{\frac{\lambda_1 + s\omega_1(1 - \omega_1)}{\lambda_1 + (1 - \omega_1)s} s + n^2\pi^2 L_D^2} \\ f_{2n} = & \sqrt{\frac{\lambda_2 + \eta_{II}s\omega_2(1 - \omega_2)}{\lambda_2 + (1 - \omega_2)\eta_{II}s} \eta_{II}s + n^2\pi^2 L_D^2} \\ A_n = & \frac{\cos n\pi z_{wD}}{2s} \\ B_n = & \frac{\left( \frac{f_{1n}}{f_{2n}} K_1(f_{1n} r_{mD}) K_0(f_{2n} r_{mD}) - \frac{1}{M_{12}} K_0(f_{1n} r_{mD}) K_1(f_{2n} r_{mD}) \right)}{\left( \frac{f_{1n}}{f_{2n}} I_1(f_{1n} r_{mD}) K_0(f_{2n} r_{mD}) + \frac{1}{M_{12}} I_0(f_{1n} r_{mD}) K_1(f_{2n} r_{mD}) \right)} \cdot \frac{\cos n\pi z_{wD}}{2s} \end{aligned}$$

Considering the storage effect and skin effect, the pseudo pressure perturbation solution can be expressed as follows:

$$\bar{\zeta}_{1wD} = \frac{s\bar{\zeta}_{1D0} + S}{s + C_D s^2 (s\bar{\zeta}_{1D0} + S)} \tag{13}$$

The dimensionless pseudo pressure for the dual medium model is expressed as follows:

$$m_{fD} = -\frac{1}{\gamma_{mD}} \ln(1 - \gamma_{mD} \bar{\zeta}_{1wD}) \tag{14}$$

## 2.2. Triple Medium Model of Composite Gas Reservoir

### 2.2.1. Physical Model

The triple-porosity is composed of the fracture, matrix, and cave. The fracture is the only channel to the wellbore, the physical properties of reservoirs in the inner and outer zone are different, but both are triple medium.

Other assumptions are consistent with Section 2.1 in [2]. The physical model is shown in Figure 2.

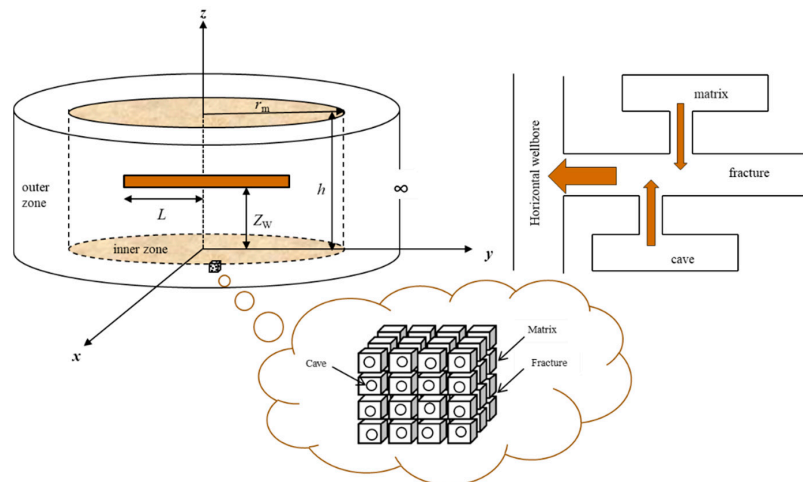


Figure 2. Physical model of triple medium composite reservoir.

### 2.2.2. Mathematical Model

Continuity equations are as follows:

$$\begin{cases} \frac{\partial(\rho_f \varphi_f)}{\partial t} + \nabla \cdot (\rho \vec{v}_f) - q_m - q_v = 0 \\ \frac{\partial(\rho_m \varphi_m)}{\partial t} + q_m = 0 \\ \frac{\partial(\rho_v \varphi_v)}{\partial t} + q_v = 0 \end{cases} \tag{15}$$

Interporosity flow equations:

$$\begin{cases} q_m = \frac{3.6\alpha K_m \rho_0}{\mu} (p_m - p_f) \\ q_v = \frac{3.6\alpha K_v \rho_0}{\mu} (p_v - p_f) \end{cases} \tag{16}$$

The fracture is the only channel, so the equation of motion is consistent with Equation (3), and we introduce the pseudo pressure Equations (5) and (17)

$$\begin{cases} m_f = \int_{p_0}^{p_f} \frac{2p}{\mu Z} dp \\ m_m = \int_{p_0}^{p_m} \frac{2p}{\mu Z} dp \end{cases} \tag{17}$$

By introducing the dimensionless equations in Table 2, the differential equations of the triple medium model can be obtained, respectively:

Inner ( $0 \leq r_D \leq r_{mD}$ ):

$$\begin{cases} \frac{1}{r_D} \frac{\partial}{\partial r_D} \left( r_D \frac{\partial m_{f1D}}{\partial r_D} \right) - \gamma_{mD} \left( \frac{\partial m_{f1D}}{\partial r_D} \right)^2 + L_D^2 \left[ \frac{\partial^2 m_{f1D}}{\partial z_D^2} - \gamma_{mD} \left( \frac{\partial m_{f1D}}{\partial z_D} \right)^2 \right] \\ = e^{\gamma_{mD} m_{f1D}} \left[ \omega_{f1} \frac{\partial m_{f1D}}{\partial t_D} + \omega_{m1} \frac{\partial m_{m1D}}{\partial t_D} + (1 - \omega_{f1} - \omega_{m1}) \frac{\partial m_{v1D}}{\partial t_D} \right] \\ \omega_{m1} \frac{\partial m_{m1D}}{\partial t_D} + \lambda_{m1} (m_{m1D} - m_{f1D}) = 0 \\ (1 - \omega_{f1} - \omega_{m1}) \frac{\partial m_{v1D}}{\partial t_D} + \lambda_{v1} (m_{v1D} - m_{f1D}) = 0 \end{cases} \tag{18}$$

Outer ( $r_{mD} \leq r_D < \infty$ ):

$$\begin{cases} \frac{1}{r_D} \frac{\partial}{\partial r_D} \left( r_D \frac{\partial m_{f2D}}{\partial r_D} \right) + L_D^2 \frac{\partial^2 m_{f2D}}{\partial z_D^2} \\ = \eta_{III} \left[ \omega_{f2} \frac{\partial m_{f2D}}{\partial t_D} + \omega_{m2} \frac{\partial m_{m2D}}{\partial t_D} + (1 - \omega_{f2} - \omega_{m2}) \frac{\partial m_{v2D}}{\partial t_D} \right] \\ \eta_{III} \omega_{m2} \frac{\partial m_{m2D}}{\partial t_D} + \lambda_{m2} (m_{m2D} - m_{f2D}) = 0 \\ \eta_{III} (1 - \omega_{f2} - \omega_{m2}) \frac{\partial m_{v2D}}{\partial t_D} + \lambda_{v2} (m_{v2D} - m_{f2D}) = 0 \end{cases} \tag{19}$$

Conditions:

$$\begin{cases} m_{fjD}|_{t_D=0} = m_{mjD}|_{t_D=0} = m_{vjD}|_{t_D=0} = 0 \quad (j = 1, 2) \\ \lim_{\varepsilon_D \rightarrow 0} \left[ \lim_{r_D \rightarrow 0^+} \int_{z_{wD} - \frac{\varepsilon_D}{2}}^{z_{wD} + \frac{\varepsilon_D}{2}} \left( r_D e^{-\gamma_{mD} m_{fD}} \frac{\partial m_{f1D}}{\partial r_D} \right) dz_{wD} \right] = -\frac{1}{2} |z_D - z_{wD}| \leq \frac{\varepsilon_D}{2} \\ m_{f1D}|_{r_D=r_{mD}} = m_{f2D}|_{r_D=r_{mD}} \\ \frac{\partial m_{f1D}}{\partial r_D} |_{r_D=r_{mD}} = \frac{1}{M_{12}} \frac{\partial m_{f2D}}{\partial r_D} |_{r_D=r_{mD}} \\ m_{f2D}|_{r_D \rightarrow \infty} = m_{m2D}|_{r_D \rightarrow \infty} = m_{v2D}|_{r_D \rightarrow \infty} = 0 \\ \frac{\partial m_{fjD}}{\partial z_D} |_{z_D=0,1} = \frac{\partial m_{mjD}}{\partial z_D} |_{z_D=0,1} = \frac{\partial m_{vjD}}{\partial z_D} |_{z_D=0,1} = 0 \quad (j = 1, 2) \end{cases} \tag{20}$$

**Table 2.** Dimensionless variables of the triple model.

Variable	Equation ( $j=1,2$ )	Variable	Equation ( $j=1,2$ )
Fracture pseudo pressure	$m_{fjD} = \frac{78.489K_{fhj}h}{Tq_{sc}} (m_i - m_{fj})$	Storage coefficient	$C_D = \frac{0.159C}{(\varphi_{f1}C_{ft1} + \varphi_{m1}C_{mt1} + \varphi_{v1}C_{vt1})hL^2}$
Matrix pseudo pressure	$m_{mjD} = \frac{78.489K_{fhj}h}{Tq_{sc}} (m_i - m_{mj})$	Fracture storage ratio	$\omega_{fj} = \frac{\varphi_{fj}C_{ftj}}{\varphi_{fj}C_{ftj} + \varphi_{mj}C_{mtj} + \varphi_{vj}C_{vtj}}$
Cave pseudo pressure	$m_{vjD} = \frac{78.489K_{fhj}h}{Tq_{sc}} (m_i - m_{vj})$	Matrix–fracture interporosity coefficient	$\lambda_{mj} = \alpha_j \frac{K_{mj}}{K_{fhj}} L^2$
Fracture storage ratio	$\omega_{fj} = \frac{\varphi_{fj}C_{ftj}}{\varphi_{fj}C_{ftj} + \varphi_{mj}C_{mtj} + \varphi_{vj}C_{vtj}}$	Cave–fracture interporosity coefficient	$\lambda_{vj} = \alpha_j \frac{K_{vj}}{K_{fhj}} L^2$
Matrix storage ratio	$\omega_{mj} = \frac{\varphi_{mj}C_{mtj}}{\varphi_{fj}C_{ftj} + \varphi_{mj}C_{mtj} + \varphi_{vj}C_{vtj}}$	Time	$t_D = \frac{3.6K_{fh1}t}{(\varphi_{f1}C_{ft1} + \varphi_{m1}C_{mt1} + \varphi_{v1}C_{vt1})\mu_1L^2}$
Cave storage ratio	$\omega_{vj} = \frac{\varphi_{vj}C_{vtj}}{\varphi_{fj}C_{ftj} + \varphi_{mj}C_{mtj} + \varphi_{vj}C_{vtj}}$	Pressure transmitting coefficient ratio	$\eta_{III} = \frac{K_{fh1}\mu_2(\varphi_{f2}C_{ft2} + \varphi_{m2}C_{mt2} + \varphi_{v2}C_{vt2})}{K_{fh2}\mu_1(\varphi_{f1}C_{ft1} + \varphi_{m1}C_{mt1} + \varphi_{v1}C_{vt1})}$

Introducing Pedrosa substitution, Laplace transform, and orthogonal transform to the model:

$$\left\{ \begin{aligned} & \frac{1}{r_D} \frac{\partial}{\partial r_D} \left( r_D \frac{\partial \bar{\bar{\xi}}_{1D0}}{\partial r_D} \right) - \left[ s \left[ \omega_{f1} + \frac{\omega_{m1}\lambda_{m1}}{\lambda_{m1} + \omega_{m1}s} + \frac{(1-\omega_{f1}-\omega_{m1})\lambda_{v1}}{\lambda_{v1} + (1-\omega_{f1}-\omega_{m1})s} \right] + n^2\pi^2L_D^2 \right] \bar{\bar{\xi}}_{1D0} = 0 \\ & \frac{1}{r_D} \frac{\partial}{\partial r_D} \left( r_D \frac{\partial \bar{\bar{m}}_{f2D}}{\partial r_D} \right) - \left[ \eta_{III}s \left[ \omega_{f2} + \frac{\omega_{m2}\lambda_{m2}}{\lambda_{m2} + \eta_{III}s\omega_{m2}} + \frac{(1-\omega_{f2}-\omega_{m2})\lambda_{v2}}{\lambda_{v2} + \eta_{III}s(1-\omega_{f2}-\omega_{m2})} \right] + n^2\pi^2L_D^2 \right] \bar{\bar{m}}_{f2D} = 0 \\ & \lim_{r_D \rightarrow 0} r_D \frac{\partial \bar{\bar{\xi}}_{1D0}}{\partial r_D} = \frac{-\cos n\pi z_w D}{2s} \\ & \bar{\bar{\xi}}_{1D0} |_{r_D=r_{mD}} = \bar{\bar{m}}_{f2D} |_{r_D=r_{mD}} \\ & \frac{\partial \bar{\bar{\xi}}_{1D0}}{\partial r_D} |_{r_D=r_{mD}} = \frac{1}{M_{f2}} \frac{\partial \bar{\bar{m}}_{f2D}}{\partial r_D} |_{r_D=r_{mD}} \\ & \bar{\bar{m}}_{f2D} |_{r_D \rightarrow \infty} = \bar{\bar{m}}_{m2D} |_{r_D \rightarrow \infty} = \bar{\bar{m}}_{v2D} |_{r_D \rightarrow \infty} = 0 \end{aligned} \right. \tag{21}$$

According to the point–source function and the properties of the Bessel function (Liu 2002; Duan 2008) [18,19], and using the definition of inverse orthogonal transformation, the zeroth–order perturbation solution in the Laplace domain can be achieved:

$$\begin{aligned} \bar{\bar{\xi}}_{1D0} = & A_0 \int_{-1}^1 K_0(F_{10}\sqrt{(x_D - \alpha)^2}) d\alpha + B_0 \int_{-1}^1 I_0(F_{10}\sqrt{(x_D - \alpha)^2}) d\alpha \\ & + 2 \sum_{n=1}^{\infty} \left[ \begin{aligned} & A_n \int_{-1}^1 K_0(F_{1n}\sqrt{(x_D - \alpha)^2}) d\alpha \\ & + B_n \int_{-1}^1 I_0(F_{1n}\sqrt{(x_D - \alpha)^2}) d\alpha \end{aligned} \right] \cdot \cos n\pi z_D \end{aligned} \tag{22}$$

where

$$\begin{aligned} F_{1n} = & \sqrt{s \left[ \omega_{f1} + \frac{\omega_{m1}\lambda_{m1}}{\lambda_{m1} + \omega_{m1}s} + \frac{(1-\omega_{f1}-\omega_{m1})\lambda_{v1}}{\lambda_{v1} + (1-\omega_{f1}-\omega_{m1})s} \right] + n^2\pi^2L_D^2} \\ F_{2n} = & \sqrt{\eta_{III}s \left[ \omega_{f2} + \frac{\omega_{m2}\lambda_{m2}}{\lambda_{m2} + \eta_{III}s\omega_{m2}} + \frac{(1-\omega_{f2}-\omega_{m2})\lambda_{v2}}{\lambda_{v2} + \eta_{III}s(1-\omega_{f2}-\omega_{m2})} \right] + n^2\pi^2L_D^2} \end{aligned}$$

According to Section 2.1.2, the dimensionless pseudo pressure of the triple medium composite reservoir with the storage effect and skin effect can also be obtained.

### 2.3. General Model

According to Equations (12) and (22) in this paper, and Equation (36) in the literature [1], it was found that the expressions of pseudo pressure of the three models were

basically the same, only the expressions of “ $\lambda_n$ ”; “ $f_n$ ”; “ $F_n$ ” were different. Therefore, a general model can be established to analyze the pressure performance of composite reservoirs with different medium types, and its bottom pseudo pressure expression is as follows:

$$\begin{aligned} \bar{\xi}_{1D0} = & A_0 \int_{-1}^1 K_0(X_{10} \sqrt{(x_D - \alpha)^2}) d\alpha + B_0 \int_{-1}^1 I_0(X_{10} \sqrt{(x_D - \alpha)^2}) d\alpha \\ & + 2 \sum_{n=1}^{\infty} \left[ \begin{array}{l} A_n \int_{-1}^1 K_0(X_{1n} \sqrt{(x_D - \alpha)^2}) d\alpha \\ + B_n \int_{-1}^1 I_0(X_{1n} \sqrt{(x_D - \alpha)^2}) d\alpha \end{array} \right] \cdot \cos n\pi z_D \end{aligned} \quad (23)$$

where:

$$A_n = \frac{\cos n\pi z_{wD}}{2s}$$

$$B_n = \frac{\left( \frac{X_{1n}}{X_{2n}} K_1(X_{1n} r_{mD}) K_0(X_{2n} r_{mD}) - \frac{1}{M_{12}} K_0(X_{1n} r_{mD}) K_1(X_{2n} r_{mD}) \right)}{\left( \frac{X_{1n}}{X_{2n}} I_1(X_{1n} r_{mD}) K_0(X_{2n} r_{mD}) + \frac{1}{M_{12}} I_0(X_{1n} r_{mD}) K_1(X_{2n} r_{mD}) \right)} \cdot \frac{\cos n\pi z_{wD}}{2s}$$

For the single medium model  $X_{1n} = \lambda_{1n}$ ,  $X_{2n} = \lambda_{2n}$ , for the dual medium model  $X_{1n} = f_{1n}$ ,  $X_{2n} = f_{2n}$ , for the triple medium model  $X_{1n} = F_{1n}$ ,  $X_{2n} = F_{2n}$ , it can make the model apply to the actual analysis more easily and flexibly.

At the same time, we found a new problem. The model listed in this paper was the case of a single medium, dual medium, or triple medium in both the inner and outer zones. However, in practice, there are also composite reservoirs with different types of medium, so the general model of Equation (23) is no longer applicable.

After further derivation, it was found that a general model of a random combination of reservoir types in the inner and outer zones can be obtained by simple transformation such as “single–dual” and “dual–triple”.

Take the “dual–triple” model as an example, and also using Equation (23) for analysis. In this case, the inner zone of the composite reservoir is dual medium and the outer zone is triple medium. Replace the inner zone  $X_{1n}$  of Equation (23) with the inner zone of the dual medium model  $f_{1n}$ , and the outer zone  $X_{2n}$  with the outer zone of the triple medium model  $F_{2n}$ , that is,  $X_{1n} = f_{1n}$ ,  $X_{2n} = F_{2n}$ . See Section 3.2 for a specific case analysis.

### 3. Results and Discussion

#### 3.1. Curve Analysis

The dimensionless pressure and pressure derivative type curves were drawn. Figures 3–5 show the pressure dynamic curves of the single medium, dual medium, and triple medium model under the influence of stress sensitivity. It can be seen that the curves of the single medium model, dual medium model, and triple medium model can be divided into seven, nine, and 13 flow stages, respectively.

Compared with the single medium model, the dual medium model had one more matrix–fracture interporosity flow stage in both the inner and outer zones (i.e., stage 5 and stage 8 in Figure 4). Compared with the dual medium model, the triple medium model had added cave–fracture interporosity flow stage and the transition flow stage after it in both the inner and outer zones (i.e., stage 5, stage 6, stage 10, and stage 11 in Figure 5).

The influence of the permeability modulus, horizontal length, skin factor, mobility ratio, radius of inner zone on pressure dynamic curve of single medium model was analyzed in [1]. Although the influence of these parameters showed some differences in the flow stage and image shape on different models, the law of influence was similar (as shown in Figures 3–5, the influence of permeability modulus on different models was similar), so it will not be repeated here.



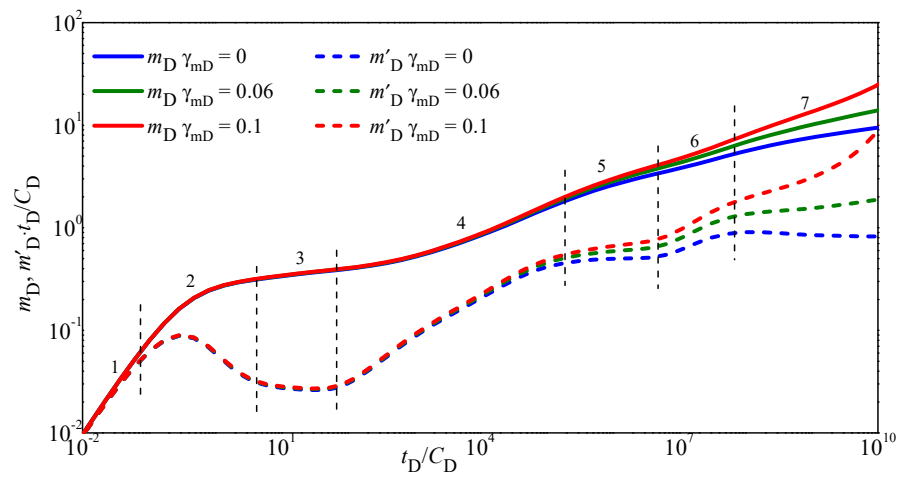


**Figure 3.** Influence of the permeability modulus on the pressure dynamic curve of a single medium composite reservoir.

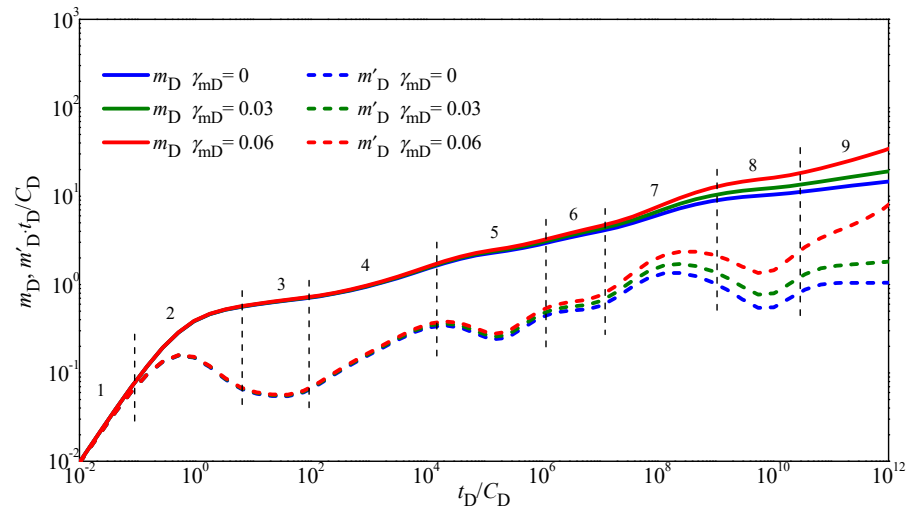


**Figure 4.** Influence of the permeability modulus on the pressure dynamic curve of the dual medium composite reservoir.

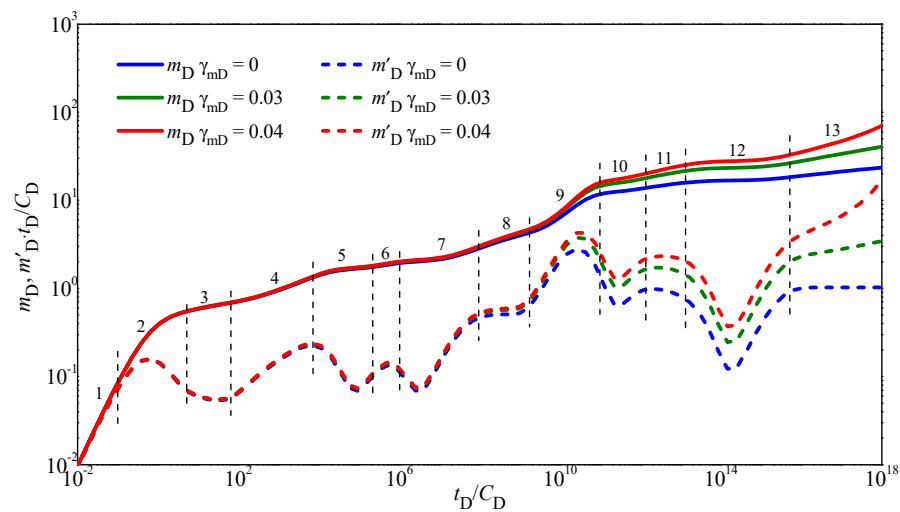


**Figure 5.** Influence of the permeability modulus on the pressure dynamic curve of the triple medium composite reservoir.

Taking the triple medium model as an example, the influence of the inner-zone cave–fracture interporosity flow coefficient; outer-zone matrix–fracture interporosity flow coefficient; inner-zone fracture storage ratio; outer-zone matrix storage ratio on the pressure dynamic curve was analyzed.

Figure 6 shows the effect of the interporosity flow coefficient between the cave and fracture of the inner zone ( $\lambda_{v1}$ ) on the derivative curve. The smaller the  $\lambda_{v1}$  means a greater difference in the flow capacity between the fracture and matrix. The flow coefficient between the cave and fracture of the outer zone ( $\lambda_{v2}$ ) on the pressure derivative type curve was mainly reflected in the first interporosity stage of the outer zone.

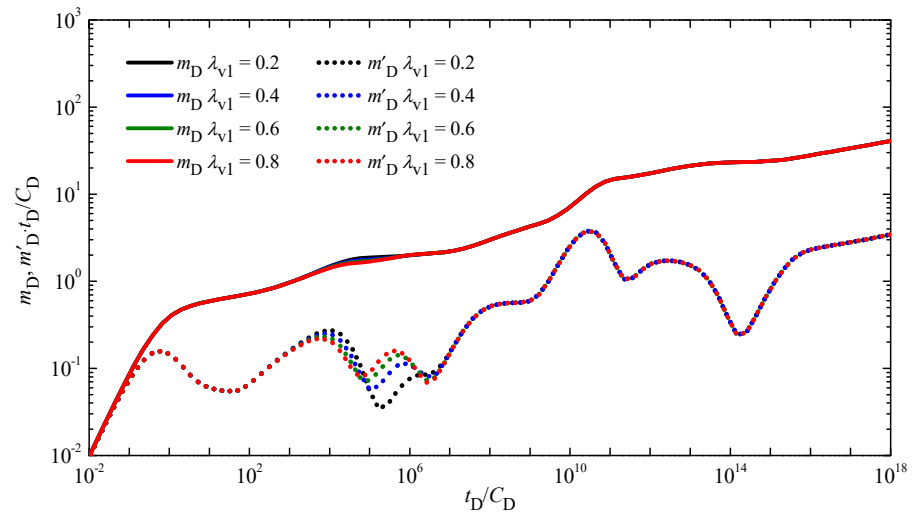


Figure 6. Influence of the inner-zone cave–fracture interporosity flow coefficient on the pressure type curve.

As demonstrated by Figure 7, the influence of the interporosity flow coefficient between the matrix and fracture of the outer zone ( $\lambda_{m2}$ ) on the pressure derivative type curve is most mirrored in stage 12. With the decrease in  $\lambda_{m2}$ , the “dip” gradually moved to the right, that the later the occurrence of the interporosity flow. This feature is similar to the influence of  $\lambda_{v1}$  on the pressure derivative type curve but at different stages. The flow coefficient between the matrix and fracture of the inner zone ( $\lambda_{m1}$ ) on the pressure derivative type curve was mainly reflected at the second inner-zone interporosity flow stage.

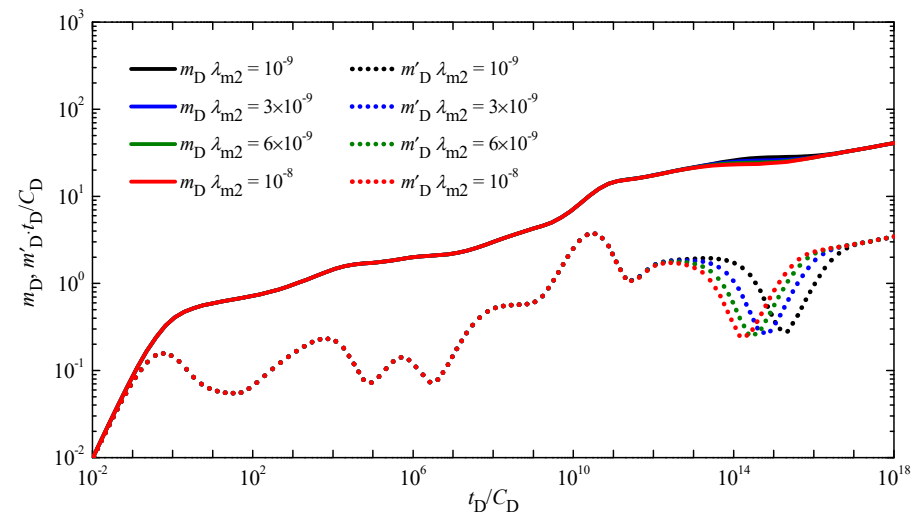


Figure 7. Influence of the outer-zone matrix–fracture interporosity flow coefficient on the pressure type curve.

As demonstrated by Figure 8, for the most part, the influence of the fracture storage ratio of the inner zone ( $\omega_{f1}$ ) on the type curve was reflected in stage 3 to stage 5. With the decrease in  $\omega_{f1}$ , the position of the pressure increased (the solid lines). In this period, with the decrease in the fracture storage ratio of the inner zone, the duration of stage 3 became shorter, and the first “dip” of the inner zone became deeper and wider (the dotted lines). Overall, the greater the fracture storage ratio of the inner zone, the shorter the duration of the interporosity flow, and the shallower the “dip”. This is because the greater fracture storage ratio means the stronger the storage capacity of the fracture system. Additionally, the effect of the fracture storage ratio of the outer zone ( $\omega_{f2}$ ) on the pressure derivative type curve was mainly reflected at the transition stage of the inner and outer zone to the first outer-zone interporosity flow stage.

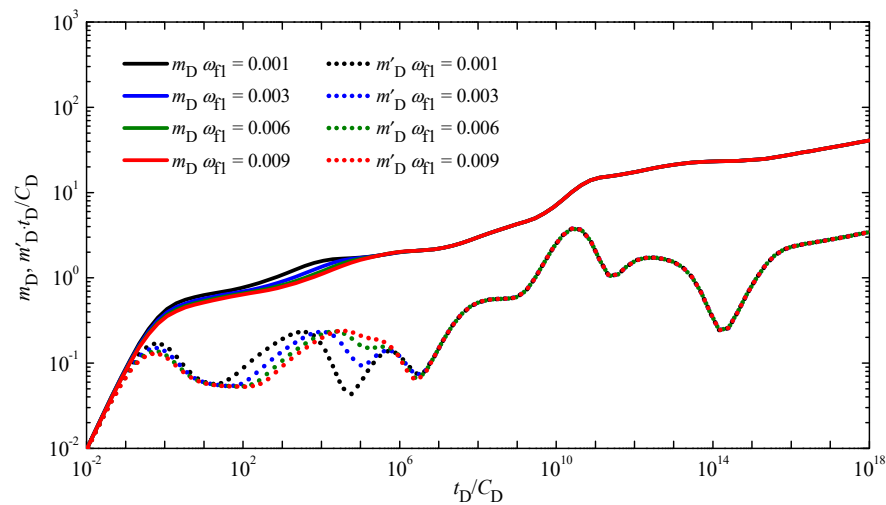


Figure 8. Influence of the inner-zone fracture storage ratio on the pressure type curve.

The influence of the matrix storage ratio of the outer zone ( $\omega_{m2}$ ) (Figure 9) on the derivative curve was most mirrored in stage 9 to stage 12. Similarly, the effect of the matrix storage ratio of the inner zone ( $\omega_{m1}$ ) on the pressure derivative type curve mainly acted on stage 5 to stage 7. With the decrease in  $\omega_{m2}$ , the first “dip” became deeper and wider, while the second “dip” became shallower and narrower (the dotted lines), and the position of the pressure decreased (the solid lines). The feature of the matrix storage ratio on the pressure curve was the opposite of that the feature of the fracture storage ratio on the pressure type curve. When the cave storage ratio is constant, the larger matrix storage ratio will cause a smaller fracture storage ratio, so they had the opposite effect on the type curve.

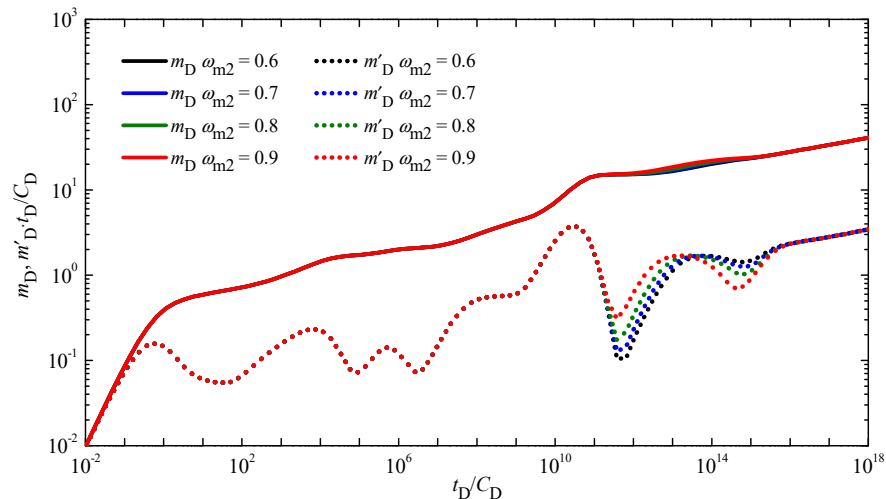
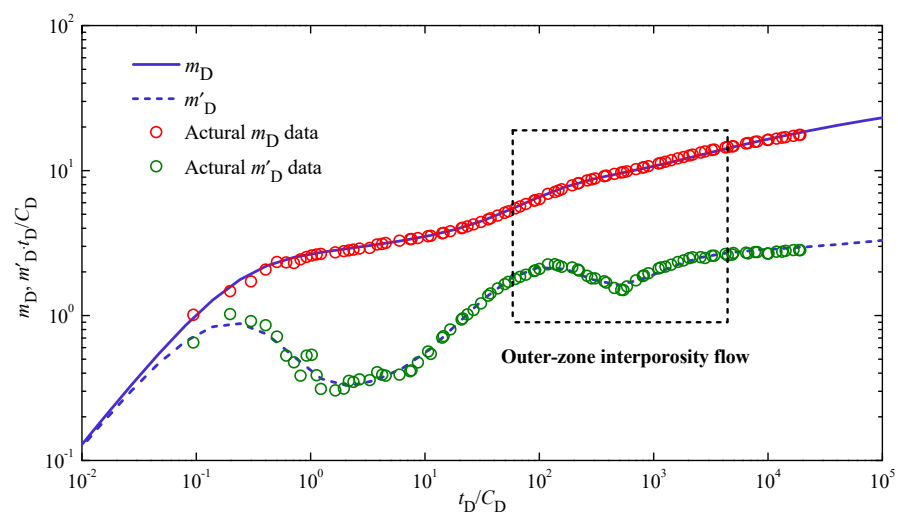


Figure 9. Influence of the outer-zone matrix storage ratio on the pressure type curve.

### 3.2. Model Validation

There is a horizontal well X1 from one carbonate gas reservoir in Central Sichuan China, where the reservoir is mainly composed of dolomite, containing quartz, feldspar, calcite, etc. Composition of natural gas: CH<sub>4</sub> content is 92.32%, CO<sub>2</sub> is 4.11%, H<sub>2</sub>S is 1.47%, and N<sub>2</sub> is 1.19%. The basic parameters are below. The average porosity is 3.82%, the thickness of the reservoir is 16 m, the well radius is 0.108 m, the gas gravity is 0.6099, the gas viscosity is 0.0206 mPa·s, the reservoir temperature is 408 K, and the initial pressure is 35.52 MPa. The well has been produced for 737 h with a rate of  $29.17 \times 10^4$  m<sup>3</sup>/d before the pressure build-up test.

As shown in Figure 10, general well testing software such as Saphir cannot fit the actual data of X1 very well, but the general model proposed in this paper could achieve better results. According to the general shape of the actual data of X1, the theoretical curve of the model with a single medium in the inner zone and dual medium in the outer zone was selected for fitting. In this case, in the general model Equation (23)  $X_{1n} = \lambda_{1n}$ ,  $X_{2n} = f_{2n}$ .



**Figure 10.** The log–log fitting curve for the X1 well.

As has been showcased in Figure 10, the variance tendency of the measured data was consistent with the pressure dynamic curve of the “single–double” medium horizontal composite model. Based on the good agreement shown in Figure 10, we argue that the presented model may offer a practical method to predict and evaluate the transient pressure behavior of a multi–medium composite reservoir. If we do not consider the characteristics of the composite reservoir, the “outer–zone interporosity flow” stage in Figure 10 cannot be fitted. The analysis results of the X1 well are listed in Table 3.

**Table 3.** The pressure transient analysis results of the X1 well.

Parameters	Value
Vertical permeability of inner zone $K_{v1}$ ( $\mu\text{m}^2$ )	$3.85 \times 10^{-4}$
Horizontal permeability of inner zone $K_{h1}$ ( $\mu\text{m}^2$ )	$6.39 \times 10^{-4}$
Skin factor $S$	0.62
Mobility ratio $M_{12}$	4.54
Outer–zone interporosity flow coefficient $\lambda_2$	0.08
Outer–zone storage ratio $\omega_2$	0.41
Inner zone radius $r_m$ (m)	177
Pseudo permeability modulus $\gamma_m$ (mPa·s/MPa <sup>2</sup> )	$0.53 \times 10^{-4}$

#### 4. Conclusions

The general model established in this paper combines the theory with the actual situation. Compared with the general gas reservoir model, it had higher accuracy and can make up for the limitations of using well testing software to obtain the formation parameters.

(1) The general model established in this paper can analyze the dynamic characteristics of pressure in composite reservoirs with an arbitrary combination of reservoir medium types, and can be applied to production practice more widely and flexibly.

(2) The typical curve of the dual medium model has two more stages than that of the single medium model in the matrix–fracture interporosity stage in both zones, and the curve of the triple medium model has four more stages than that of the dual medium model in the cave–fracture interporosity stage and the transition flow stage in both zones.

(3) The effect of stress sensitivity on the later stage of the typical curve is more significant because the stronger the stress sensitivity, the greater the damage to the reservoir and the greater the differential pressure required. The interporosity coefficient represents the flow ability of the reservoir, where the smaller the parameter, the weaker the flow ability, which causes a greater the difference between each medium, and later, the channeling occurs. The elastic storage capacity ratio represents the reservoir capacity of the fractures, where the larger it is, the stronger the fracture capacity and the shorter the crossflow duration.

#### 5. Suggestions

(1) The models derived in this paper were all based on the two–layer composite reservoir. If special reservoirs are encountered in the process of exploitation, a multi zone composite reservoir model can be deduced. However, it is not recommended to blindly study larger numbers of zones because it is impractical and of little significance.

(2) The unsteady pressure dynamic curve of the composite gas reservoir with an arbitrary medium type combination can be predicted by referring to the changes in Figures 3–5 in this paper. However, it should be noted that the theoretical curve may not reflect all of the flow stages, especially for the reservoirs with more than two zones.

(3) The research objects of this paper were all horizontal wells. We suggest an unsteady seepage model of a composite gas reservoir with fractured horizontal wells in further study.

**Author Contributions:** Methodology, Y.H.; Validation, Y.H. and X.L.; Formal analysis, Y.H., M.M. and X.W.; Resources, Y.H. and X.L.; Data curation, Y.H., M.M. and X.W.; Writing—original draft preparation, Y.H.; Writing—review and editing, M.M. and X.W.; Funding acquisition, Y.H. All authors have read and agreed to the published version of the manuscript.

**Funding:** This research was funded by the General Program of the Chongqing Natural Science Foundation (grant number: cstc2020jcyj–msxmX0660, cstc2020jcyj–msxmX0174), and the Science and Technology Research Project of Chongqing Education Commission (grant number: KJQN202001535).

**Data Availability Statement:** Not applicable.

**Conflicts of Interest:** The authors declare no conflict of interest regarding the publication of this paper.

#### Nomenclature

$C$	Wellbore storage coefficient, $\text{m}^3/\text{MPa}$
$C_D$	Dimensionless wellbore storage coefficient
$C_t$	Total compressibility coefficient, $\text{MPa}^{-1}$
$h$	Reservoir thickness, m
$h_D$	Dimensionless reservoir thickness
$K_v$	Vertical permeability, $\mu\text{m}^2$
$K_h$	Horizontal permeability, $\mu\text{m}^2$
$L$	Horizontal section length, m
$L_D$	Dimensionless horizontal section length

$m$	Pseudo pressure, $\text{MPa}^2/(\text{mPa}\cdot\text{s})$
$m_D$	Dimensionless pseudo pressure
$r$	Radial distance, m
$r_D$	Dimensionless radial distance
$z$	Vertical distance, m
$z_D$	Dimensionless vertical distance
$z_w$	Horizontal section position, m
$z_{wD}$	Dimensionless horizontal section position
$p$	Pressure, MPa
$p_i$	Initial formation pressure, MPa
$T$	Absolute temperature, K
$Z$	Gas deviation factor
$s$	Laplace transform variable
$S$	Skin factor, dimensionless
$t$	Time, hours
$t_D$	Dimensionless time
$\varepsilon$	Tiny variable
$\gamma_m$	Pseudo-permeability modulus, $\text{mPa}\cdot\text{s}/\text{MPa}^2$
$\gamma_{mD}$	Dimensionless pseudo-permeability modulus
$\mu$	Gas viscosity, $\text{mPa}\cdot\text{s}$
$\rho$	Gas density, $\text{kg}/\text{m}^3$
$\varphi$	Porosity, fraction
$\lambda_m$	Interporosity flow coefficient between matrix and fracture, dimensionless
$\lambda_v$	Interporosity flow coefficient between cave and fracture, dimensionless
$\omega_f$	Storage ratio, fraction
$\omega_m$	Matrix storage ratio, fraction
$\omega_v$	Cave storage ratio, fraction
Subscripts:	
D	Dimensionless
f	Fracture
m	Matrix
v	Cave
$j$	1, 2 (1 = inner zone, 2 = outer zone)

## References

- Liu, E.B.; Peng, Y.; Peng, S.B.; Yu, B.; Chen, Q.K. Research on low carbon emission optimization operation technology of natural gas pipeline under multi-energy structure. *Pet. Sci.* **2022**. [\[CrossRef\]](#)
- Huang, Y.; Li, X.; Tan, X. Transient Pressure and Rate Decline Analysis for Horizontal Well in Stress-Sensitive Composite Reservoir. *Math. Probl. Eng.* **2018**, *2018*, 8672578. [\[CrossRef\]](#)
- Fatt, I.; Davis, D.H. Reduction in Permeability with Overburden Pressure. *J. Pet. Technol.* **1952**, *4*, 16. [\[CrossRef\]](#)
- Pedrosa, O.A. Pressure Transient Response in Stress-Sensitive Formations. In Proceedings of the SPE California Regional Meeting, Oakland, CA, USA, 2–4 April 1986.
- Warren, J.E. The behavior of naturally fractured reservoirs. *Soc. Pet. Eng. J.* **1963**, *3*, 245–255. [\[CrossRef\]](#)
- Closmann, P.J. Aquifer model for fissured reservoirs. *Soc. Pet. Eng. J.* **1975**, *15*, 385–398. [\[CrossRef\]](#)
- Jiang, L.; Liu, J.; Liu, T.; Yang, D. Semi-analytical modeling of transient pressure behaviour for a fractured vertical well with hydraulic/natural fracture networks by considering stress-sensitive effect—ScienceDirect. *J. Nat. Gas Sci. Eng.* **2020**, *82*, 103477. [\[CrossRef\]](#)
- Lu, J.; Rahman, M.M.; Yang, E.; Alhamami, M.T.; Zhong, H. Pressure transient behavior in a multilayer reservoir with formation crossflow. *J. Pet. Sci. Eng.* **2022**, *208*, 109376. [\[CrossRef\]](#)
- Zhao, Y.L.; Zhang, L.H.; Zhao, J.Z.; Luo, J.X.; Zhang, B.N. “Triple porosity” modeling of transient well test and rate decline analysis for multi-fractured horizontal well in shale gas reservoirs. *J. Pet. Sci. Eng.* **2013**, *110*, 253–262. [\[CrossRef\]](#)
- Guo, J.; Zhang, L.; Zhu, Q. A quadruple-porosity model for transient production analysis of multiple-fractured horizontal wells in shale gas reservoirs. *Environ. Earth Sci.* **2015**, *73*, 5917–5931. [\[CrossRef\]](#)
- Chen, L.; Liu, Y.; Zhu, Z.; Gao, D.; Cao, W.; Li, Q. The discrete numerical model and transient pressure curves of fractured-vuggy units in carbonate reservoir. *Sci. Technol. Rev.* **2017**, *35*, 89–95.
- Li, W.; Li, S.; Zhang, S.; Dong, X.; Fan, Q. Application of a constructive method in solving the composite reservoir model of dual-porosity media with fractal characteristics. *J. Pet. Sci. Eng.* **2021**, *208*, 109702. [\[CrossRef\]](#)

13. Meng, F.; Lei, Q.; He, D.; Yan, H.; Jia, A.; Deng, H.; Xu, W. Production performance analysis for deviated wells in composite carbonate gas reservoirs. *J. Nat. Gas Sci. Eng.* **2018**, *56*, 333–343. [[CrossRef](#)]
14. Zhao, Y.L.; Xie, S.C.; Peng, X.L.; Zhang, L.H. Transient pressure response of fractured horizontal wells in tight gas reservoirs with arbitrary shapes by the boundary element method. *Environ. Earth Sci.* **2016**, *75*, 1220. [[CrossRef](#)]
15. Wu, M.; Ding, M.; Yao, J.; Xu, S.; Li, L.; Li, X. Pressure transient analysis of multiple fractured horizontal well in composite shale gas reservoirs by boundary element method. *J. Pet. Sci. Eng.* **2017**, *162*, 84–101. [[CrossRef](#)]
16. Zhu, L.; Liao, X.; Chen, Z. Pressure Transient Analysis of Vertically Fractured Well in Tight Oil Reservoirs with Rectangle Stimulated Reservoir Volume. In Proceedings of the SPE Kingdom of Saudi Arabia Annual Technical Symposium and Exhibition, Dammam, Saudi Arabia, 24–27 April 2017.
17. Wang, M.; Fan, Z.; Xing, G.; Zhao, W.; Song, H.; Su, P. Rate Decline Analysis for Modeling Volume Fractured Well Production in Naturally Fractured Reservoirs. *Energies* **2018**, *11*, 43. [[CrossRef](#)]
18. Liu, S. *Special Functions*; Meteorological Press: Beijing, China, 2002; pp. 386–427.
19. Duan, Z. *Equations of Mathematical Physics & Special Functions*; Higher Education Press: Beijing, China, 2008; pp. 119–128.